


Cite this: *J. Mater. Chem. A*, 2017, 5, 10651

Freestanding nano-photoelectrode as a highly efficient and visible-light-driven photocatalyst for water-splitting†

Yansong Zhou,^a Gang Chen,^b *^a Edward H. Sargent,^b Taotao Zhuang,^b Cao Thang Dinh^b and Fang He^a

Solar energy conversion through artificial photosynthesis is of considerable interest. Unfortunately, the efficiencies of current photocatalysts are limited by the rapid recombination of photogenerated charge carriers and their failure to respond to the long-wavelength light region in sunlight. To harness solar energy efficiently, we propose, for the first time, the concept of freestanding nano-sized photoelectrodes as efficient photocatalysts for artificial photosynthesis applications. Through introducing charge transporting components and incorporating photoactive narrow bandgap semiconductors, a long wavelength responding and freestanding nano-photoelectrode composed of PEDOT:PSS/CdS/ZnO/WS₂ has been fabricated. This freestanding nano-photoelectrode can serve as a highly efficient and stable photocatalyst for hydrogen (H₂) evolution with a rate of as high as 1028 μmol h⁻¹, without loading any noble metal containing co-catalyst, under simulated sunlight irradiation. Impressively, the designed nano-photoelectrode shows an outstanding apparent quantum efficiency (APQ) of 0.3% for H₂ evolution at a wavelength of λ = 600 nm.

Received 25th March 2017
Accepted 2nd May 2017DOI: 10.1039/c7ta02626a
rsc.li/materials-a

Introduction

Converting abundant solar energy into chemical energy through artificial photocatalytic water-splitting is one of the most promising approaches to mitigate environmental and energy issues. The photocatalytic process on semiconductor powders in a suspension system has long been a hot research topic, since it's the simplest of the solar energy conversion technologies.¹ To date, numerous candidate materials such as CDots-C₃N₄ and CoO have been demonstrated as efficient photocatalysts for water-splitting.²⁻⁵ Unfortunately, the photocatalytic activities of currently available photocatalysts are usually limited by the fast recombination of photogenerated carriers in a single material.^{6,7} To overcome this problem, the structural design of photocatalytic systems to spatially separate the photogenerated electrons and holes has been intensively investigated recently.^{4,8,9} Although numerous outstanding research has been reported,¹⁰⁻¹⁴ the

current efficiency of artificial photosynthesis fails to meet the requirements for further practical applications.

A compositing strategy has been demonstrated as an efficient strategy to suppress photogenerated electron and hole recombination in photocatalysts.¹⁵⁻¹⁷ Unfortunately, two component composited photocatalysts are always limited by the wide bandgap of the semiconductor, resulting in a failure to utilize long-wavelength light. Recently, Yu and co-workers incorporated Cu_{2-x}S¹⁸ or Au¹⁹ in a novel 1D colloidal hetero-nanostructure for enhanced solar energy conversion. Localized surface plasmon resonance in Cu_{2-x}S or Au enables effective long wavelength absorption. Although a number of photocatalysts have been reported to be able to respond to long wavelength light, most of them show rather low activity or are even not active for water-splitting under long wavelength light illumination. Currently, the rational design of semiconductor-based hetero-structures as highly efficient photocatalysts remains challenging.

Compared to powder photocatalysts, which are randomly suspended in the reacting media, the photoelectrodes of photoelectrochemical (PEC) cells are usually a set of combined films of photoactive layers, charge-transporting layers and redox catalysts that can be designed in an ordered fashion²⁰⁻²² (Fig. 1a). This rationally ordered structure makes it possible to realize efficient charge carrier separation in the photoelectrodes, resulting in promising solar energy conversion efficiency.^{23,24} However, photoelectrodes are only based on macroscopically thin films, which limits the further

^aMIIT Key Laboratory of Critical Materials Technology for New Energy Conversion and Storage, School of Chemistry and Chemical Engineering, Harbin Institute of Technology, 92 West Dazhi Street, Nan Gang District, Harbin, 150001, P. R. China. E-mail: gchen@hit.edu.cn

^bDepartment of Electrical and Computer Engineering, University of Toronto, 35 St George Street, Toronto, Ontario M5S 1A4, Canada

† Electronic supplementary information (ESI) available: Experimental details, SEM and TEM images, XRD pattern, UV-vis and PL spectra, photocatalytic performance and photoelectrochemistry characterization. See DOI: 10.1039/c7ta02626a

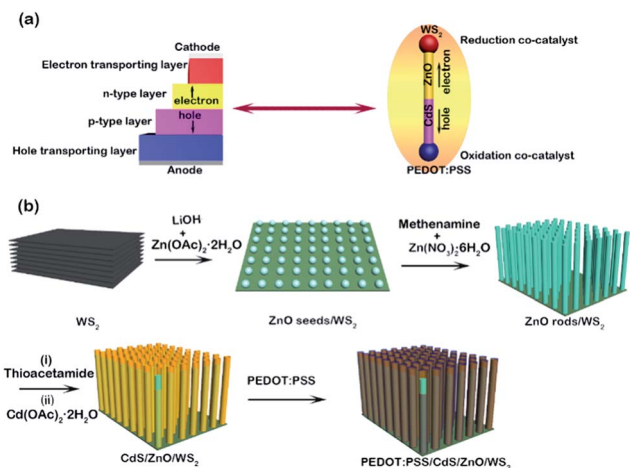


Fig. 1 (a) Structural comparison of a photovoltaic cell and the designed nano-photoelectrode. (b) Illustration of the fabrication process for the nano-photoelectrode.

enhancement of the solar energy conversion efficiency due to a lower surface reactive area and poorer mass transfer in comparison with suspended powders. Inspired by this, it is expected that designing freestanding nano-sized photoelectrodes through combining the advantages of photoelectrodes and nanotechnology would help realize highly efficient photocatalysts. Pioneering work on freestanding Pt/Si/Ag photoelectric nanodevices with exceptional photocatalytic properties was reported by Duan and coworkers,²⁵ suggesting the concept of constructing nano-sized photoelectric devices for artificial photosynthesis applications. So far, there are no other reports on the construction of photoelectric nanodevices as photocatalysts. In addition, the current synthetic approaches to photoelectric devices are complex and costly. Thus, the rational design and development of nano-sized photoelectrodes for solar energy conversion through facile methods is of great significance.

Herein, we describe, for the first time, a facile wet chemical route for the synthesis of a freestanding nano-photoelectrode for use as a highly efficient and long wavelength responding photocatalyst. CdS sensitized ZnO nanorod arrays are chosen as photoactive components, and are grown on a WS₂ nanosheet substrate to form multi-junction structures (Fig. 1a). WS₂ is chosen as the electron collection component, as well as the long wavelength light photoactive absorber, because WS₂ has been demonstrated to be an efficient co-catalyst for H₂ evolution^{26–28} and a long wavelength responding photocatalyst.^{29,30} Poly(3,4-ethylenedioxythiophene) polystyrene sulfonate (PEDOT:PSS), the most widely used hole-transporting material in polymer solar cells,³¹ is coated on the CdS surface to facilitate photo-generated hole transfer in this system, as the generated holes are quickly transferred from CdS to the polymer surface and they eventually react with the hole scavenger. The resulting freestanding PEDOT:PSS/CdS/ZnO/WS₂ nano-photoelectrode shows high and stable performance for photocatalytic H₂ evolution from water splitting under simulated sunlight irradiation. More importantly, the as-obtained nano-

photoelectrode is active for photocatalytic H₂ evolution even up to $\lambda = 600$ nm with an AQY of about 0.3%, which is a promising performance compared to the limited numbers of near-infrared light active photocatalysts for water splitting. In addition, enhanced photoelectrochemical (PEC) signals are also observed at $\lambda = 700$ nm, suggesting potential PEC applications in the near-infrared light region.

Results and discussion

In this work, PEDOT:PSS(x)/CdS(y)/ZnO/WS₂(z) is abbreviated as P(x)/C(y)/Z/W(z), in which *x*, *y* and *z* correspond to the molar or mass ratio of each component (detailed information can be found in the Experimental section). The carrier dynamics among semiconductor interfaces (or junctions) represent a key determining factor in PEC cell performance.³² To achieve well-connected interfaces among the components, a PEDOT:PSS/CdS/ZnO/WS₂ nano-photoelectrode was synthesized through a wet chemical synthesis method, combining seed-mediated growth and ion-exchange (Fig. 1b). ZnO nanoarrays were grown on a WS₂ nanosheet substrate *via* a seed-mediated growth method from ZnO nanoseeds/WS₂ (Fig. S1†). After

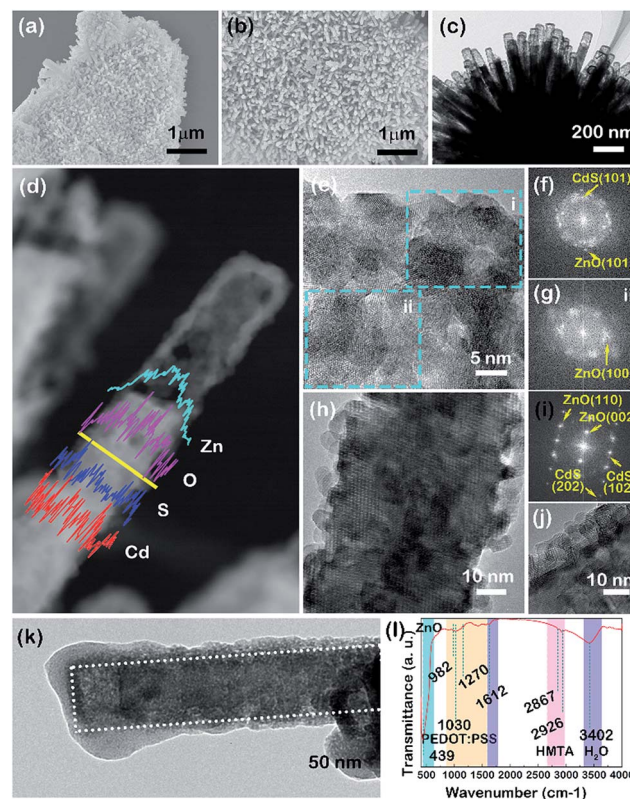


Fig. 2 (a and b) SEM images, (c) a TEM image and (d) a HAADF image (inset shows the EDS line scan profiles) of C(0.6)/Z/W(10). (e) A HRTEM image of the hollow corner. (f and g) SAED patterns corresponding to the selected area in (e). (h) A HRTEM image of the solid part of the rod and its corresponding (i) FFT image. A HRTEM image of the edge of the rod shows the clear interface. (j) A TEM image of the outer part of the nanorod. (k) A TEM image of P(1.0)/C(0.6)/Z/W(10) and its (l) FT-IR spectrum.

surface sulfidation and ion-exchange processes, ZnO nanoarrays on WS₂ nanosheets were covered in CdS to form a photoelectrode-like structure (Fig. 2a, b and S2†). X-ray diffraction (XRD) results further confirm the existence of CdS, ZnO and WS₂ phases in the sample (Fig. S3†). Nanoarrays with a uniform diameter of around 50 nm are observed in the transmission electron microscopy (TEM) images (Fig. 2c). In addition, energy dispersive X-ray spectroscopy (EDX) analysis implies the existence of WS₂, further suggesting that the nanoarrays are grown on the WS₂ nanosheet substrate (Fig. S4†). All the nanorods exhibit a hollow structure with rough surfaces (Fig. 2c). The detailed structures of the nanorods are further confirmed *via* high magnification high-angle annular dark-field (HAADF) analysis (Fig. 2d and S5†). The hollow structure of the nanorod is found to be composed of nanocrystals (Fig. 2e). Selected area electron diffraction (SAED) patterns of the outer and inner parts reveal that the outer part is a mixture of CdS and ZnO (Fig. 2f), while the inner part is mainly a ZnO phase (Fig. 2g), which is in good agreement with the EDX line scan results (Fig. S6†). A high-resolution transmission electron microscopy (HRTEM) image of the solid part is also shown in Fig. 2h, in which a single-crystal core covered in a nanocrystalline shell is observed. The corresponding SAED pattern displays two sets of diffraction spots (Fig. 2f), belonging to wurtzite-structured CdS (JCPDS no. 77-2306) and wurtzite-structured ZnO (JCPDS no. 36-1451). The results of the EDX line scan reveal that the core is mainly composed of Zn and O, while the outer part is Cd and S (Fig. 2d), suggesting that the core is ZnO and the shell is CdS. Lattice fringes corresponding to the (001) plane of ZnO, with a measured *d*-spacing of 0.52 nm, were observed for the ZnO core, indicating a crystalline ZnO nanorod growing along the ZnO [001] direction (Fig. S7†). Furthermore, a tightly contacting interface with a clear crystal lattice between CdS and ZnO is clearly observed in Fig. 2j, which would lead to strong interactions and consequently facilitate effective interband charge transfer from CdS to ZnO in the photoelectrode. When further coated with the PEDOT:PSS component, an amorphous phase covering the rods is clearly distinguishable in the TEM image (Fig. 2k). Particularly, the hollow side tends to adsorb much more PEDOT:PSS than the solid part, which is possibly due to the stronger adsorption capability of the hollow structure. Characteristic peaks at 941 cm⁻¹, 1030 cm⁻¹ and 1269 cm⁻¹ attributed to PEDOT:PSS in the FT-IR spectrum of P(1.0)/C(0.6)/Z/W(10) confirm the existence of a PEDOT:PSS component in the architectural structure (Fig. 2i),^{33,34} which is further demonstrated in the Raman results (Fig. S8†). Therefore, a freestanding nano-photoelectrode composed of PEDOT:PSS/CdS/ZnO/WS₂, has been fabricated.

The effects of each component on the photocatalytic H₂ evolution performance were investigated (Fig. S9†). CdS(0.6)/ZnO (C(0.6)/Z) was chosen as the base material for constructing the CdS/ZnO/WS₂ systems since the C(0.6)/Z sample showed the highest photocatalytic H₂ evolution rate, 124 μmol h⁻¹ g⁻¹, of the CdS(*x*)/ZnO (*x* = 0, 0.2, 0.4, 0.6, 0.8 and 1.0) (C(*x*)/Z) samples. When coupled with WS₂, the H₂ evolution rate was increased to 506 μmol h⁻¹ over the CdS(0.6)/ZnO/WS₂(10) (C(0.6)/Z/W(10)) sample with an optimized amount of WS₂

among the CdS(0.6)/ZnO/W(*y*) (*y* = 0, 5, 10, 15 and 20) samples. Surprisingly, the C(0.6)/Z/W(10) sample shows a much higher H₂ evolution rate than the noble metal Pt (1 wt%) loaded on the C(0.6)/Z sample, suggesting that WS₂ is an efficient H₂ evolution co-catalyst in this system. When an optimized amount of PEDOT:PSS is coated on C(0.6)/Z/W(10), the H₂ evolution rate is dramatically increased to 1028 μmol h⁻¹ (P(1.0)/CdS(0.6)/ZnO/W(10)), which is comparable to the H₂ evolution rate from PdS (1 wt%), showing that this is an efficient co-catalyst for the oxidation reaction with a metal sulfide photocatalyst³⁵ loaded CdS(0.6)/ZnO/W(10) sample. Fig. 3a presents a direct comparison of the H₂ evolution performance over pristine ZnO, ZnO/WS₂(10), C(0.6)/Z, C(0.6)/Z/W(10) and P(1.0)/C(0.6)/Z/W(10). Pristine WS₂ shows no detectable performance under the same experimental conditions. Pristine ZnO and CdS show relatively low performances. Interestingly, the P(1.0)/C(0.6)/Z/W(10) sample shows the highest photocatalytic performance, which is about 150 and 31 times higher respectively than that of ZnO or CdS without loading with any noble metal containing co-catalyst. Otherwise, the photocatalytic performance of CdS/ZnO/WS₂ and PEDOT:PSS/CdS/ZnO/WS₂ is better than the reported results based on CdS/ZnO hetero-nanostructured photocatalysts (Table S1†), indicating the advantages of the selected components and constructed structure shown in this work. CdS/WS₂(10) and P(1.0)/C(0.6)/Z were also investigated as

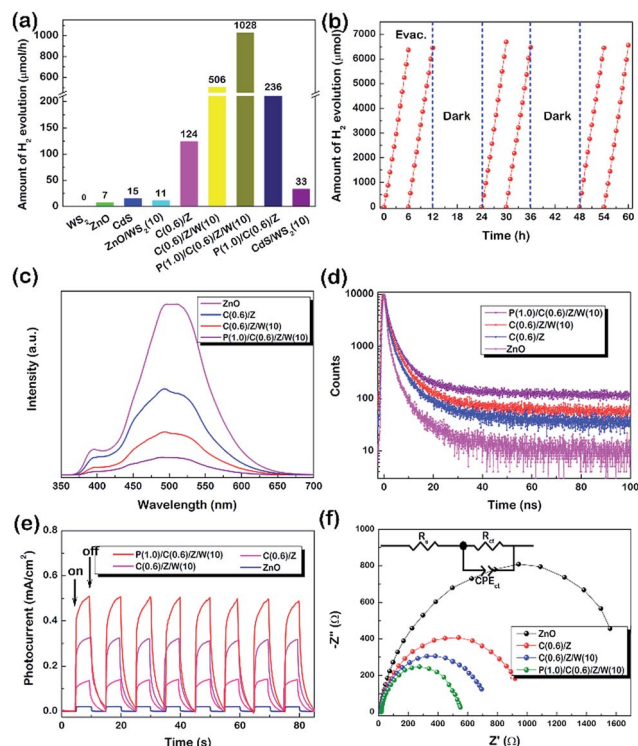


Fig. 3 (a) The photocatalytic H₂ evolution performance of the freestanding photoelectrode catalyst and controlled samples under simulated sunlight irradiation (100 mW cm⁻²). (b) The time course of photocatalytic H₂ evolution over P(1.0)/C(0.6)/Z/W(10). (c) PL spectra, (d) time-resolved photo-luminescence (TRPL) spectra, (e) photocurrents and (f) EIS plots for ZnO, C(0.6)/Z, C(0.6)/Z/W(10) (inset: the corresponding equivalent circuit), and P(1.0)/C(0.6)/Z/W(10).

references, whose performances are also far below that of the P(1.0)/C(0.6)/Z/W(10) sample. These results suggest that the rational construction and assembly of each component in the PEDOT:PSS/CdS/ZnO/WS₂ sample play a key role in achieving high photocatalytic performance. Significantly, the P(1.0)/C(0.6)/Z/W(10) sample also shows highly stable and efficient photocatalytic performance over a period of 60 h (Fig. 3b). It is widely accepted that CdS-based photocatalysts or photoanodes always suffer from photocorrosion reactions, which lead to a dramatically decrease in performance. To protect CdS from photocorrosion, different kinds of protective layers have been developed.^{36–38} In this work, PEDOT:PSS acts as an efficient protective layer for CdS, resulting in the high stability of the as-prepared nano-photoelectrode. After testing for a long time, the characteristic peaks of PEDOT:PSS at 941 cm⁻¹, 1030 cm⁻¹ and 1269 cm⁻¹ remain in the FTIR spectrum of the sample (Fig. S10†), suggesting that PEDOT:PSS is stable during the photocatalytic process. All these outcomes indicate the excellent performance and stability of this freestanding PEDOT:PSS/CdS/ZnO/WS₂ nano-photoelectrode for H₂ generation.

In order to investigate the charge carrier separation behavior in the freestanding nano-photoelectrode, photoluminescence (PL) and time-resolved photo-luminescence (TRPL) (Fig. 3c, d and S11†) spectroscopy were carried out. Charge carriers are easily transferred from CdS to ZnO due to their compatible lattice structures and proper band alignment. This is also confirmed from the decreased PL intensity and the prolonged lifetime of the charge carriers. When further composited with the electron collecting component WS₂, and the hole transporting component PEDOT:PSS, the photogenerated charge carriers are further efficiently separated. Such charge separation behaviour is also verified from the photocurrent measurements, which exhibit a similar trend to the PL data (Fig. 3e and S12†). The kinetics of interfacial charge migration in this freestanding nano-photoelectrode were further investigated using electrochemical impedance spectroscopy (EIS) (Fig. 3f). A smaller arc radius corresponds to more effective separation of photo-generated electron-hole pairs and a higher efficiency of charge migration across the electrode/electrolyte interface. The arc radius of P(1.0)/C(0.6)/Z/W(10) is the smallest among these samples (Table S2†), indicating that the rationally assembled nano-electrode structure induces charge separation and migration more efficiently, which is in good agreement with the results from the PL and photocurrent measurements.

Fig. 4a presents the UV-vis spectra of ZnO, C(0.6)/Z, C(0.6)/Z/W(10) and P(1.0)/C(0.6)/Z/W(10). ZnO alone can only respond to ultra-violet light. When sensitized with CdS, its optical absorption edge is extended to the visible light region (Fig. S13†). A similar trend is also observed when changing the CdS content in CdS/ZnO/WS₂, indicating that the existence of WS₂ has little effect on the content of CdS. The CdS(0.6)/ZnO/W(y) samples show the capability to absorb the whole visible light region, which originates from WS₂, whose optical absorption edge is up to the near-infrared light region (Fig. S14†). In addition, the optical absorption edge of PEDOT:PSS is around 350 nm (Fig. S15†), indicating the weak light shielding effects of PEDOT:PSS on other components. The

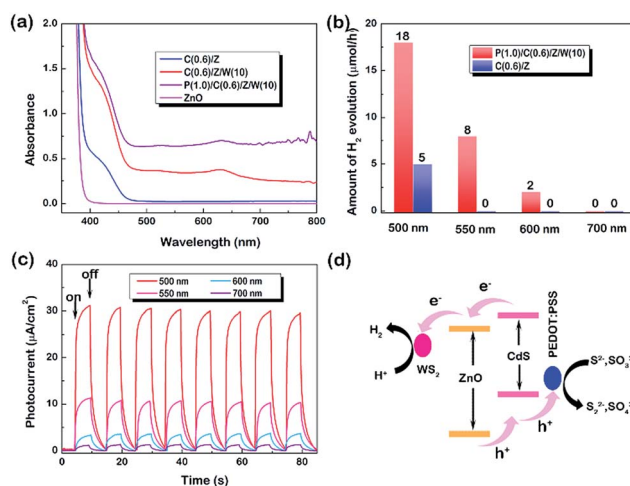


Fig. 4 (a) UV-vis spectra of ZnO, C(0.6)/Z, C(0.6)/Z/W(10) and P(1.0)/C(0.6)/Z, C(0.6)/Z/W(10). (b) Photocatalytic H₂ evolution over P(1.0)/C(0.6)/Z/W(10) and C(0.6)/Z as a function of incident light wavelength and (c) the corresponding photocurrent density over P(1.0)/C(0.6)/Z/W(10). (d) A schematic illustration of the photocatalytic mechanism over the PEDOT:PSS/CdS/ZnO/WS₂ nano-photoelectrode.

conversion of long wavelength light to chemical energy is highly desirable for artificial photocatalytic processes. In this work, the photocatalytic H₂ activity was evaluated under light with wavelengths of 500, 550, 600 and 700 nm (Fig. 4b). It's found that the P(1.0)/C(0.6)/Z/W(10) sample is active for H₂ evolution even under 600 nm illumination, with a APQ of about 0.3%. However, no H₂ was detected for C(0.6)/Z when the light wavelength was longer than 550 nm. Long wavelength PEC measurements were also carried out to further confirm the activity of the catalyst (Fig. 4c). A very weak photocurrent for C(0.6)/Z is detected up to 550 nm, while dramatically enhanced photocurrent signals are observed for the P(1.0)/C(0.6)/Z/W(10) sample under the same conditions (Fig. S16†). A significantly enhanced photocurrent signal is also observed for P(1.0)/C(0.6)/Z/W(10), even under $\lambda = 700$ nm light irradiation. In addition, WS₂ is photoactive and can generate a weak photocurrent under all these light illumination wavelengths (Fig. S17†). Since PEDOT:PSS is not photoactive for the photocatalytic and photoelectric chemical processes, the signal at $\lambda = 700$ nm is mainly attributed to photogenerated charges from WS₂, indicating that WS₂ in the PEDOT:PSS/CdS/ZnO/WS₂ nano-photoelectrode not only works as an efficient co-catalyst for H₂ evolution, but also as a long wavelength photoactive component. All these results suggest that a freestanding nano-photoelectrode with highly efficient and long wavelength responding H₂ evolution performance has been constructed.

Based on the above results, the photocatalytic mechanism and charge transfer processes in the PEDOT:PSS/CdS/ZnO/WS₂ photocatalytic systems are illustrated in Fig. 4d. Upon photo-excitation, photogenerated electrons in the conduction band of CdS and ZnO transfer to WS₂ and reduce the proton to hydrogen. Photogenerated holes transferred in the valence bands of ZnO and CdS will transfer step by step and be trapped by PEDOT:PSS. As a result, the photogenerated holes and

electrons in the freestanding nano-photoelectrodes are efficiently separated, which leads to the eventually enhanced photocatalytic performance.

Conclusions

In summary, we have constructed freestanding nano-photoelectrodes as highly efficient photocatalysts for artificial photosynthesis applications. By rationally designing and assembling photoactive and charge transporting components, a freestanding nano-photoelectrode, PEDOT:PSS/CdS/ZnO/WS₂, for photocatalytic H₂ evolution has been constructed *via* a facile wet chemical method. More importantly, the freestanding nano-photoelectrode can drive H₂ evolution at wavelengths up to $\lambda = 600$ nm. We believe that the concept and design of a freestanding nano-photoelectrode described here open up a new avenue for developing efficient photocatalysts in the field of renewable solar fuel production.

Experimental section

Chemicals

Chemical reagents including Zn(OAc)₂·2H₂O (Sinopharm Chemical Reagent Co., Ltd), LiOH (Aladdin Chemistry Co. Ltd), hexamethylenetetramine (Aladdin Chemistry Co. Ltd), Zn(NO₃)₂·6H₂O (Sinopharm Chemical Reagent Co., Ltd), WS₂ (Aladdin Chemistry Co. Ltd), thioacetamide (Sinopharm Chemical Reagent Co., Ltd), Cd(OAc)₂·2H₂O (Sinopharm Chemical Reagent Co., Ltd), PEDOT:PSS (OE Chemicals), Na₂S·9H₂O (West Long Chemical Co. Ltd), and Na₂SO₃ (Sinopharm Chemical Reagent Co., Ltd) were used without further treatment.

Sample preparation

Preparation of ZnO nanorods, CdS/ZnO nanorod composites and CdS. For ZnO seed preparation, 10 mg of ZnZn(OAc)₂·2H₂O and 10 mg of LiOH were added into 50 mL of ethanol under stirring for 10 min. After that, the mixture was put into a sonic bath (200 W) for 2 h. The ZnO seeds were collected *via* centrifugation.

ZnO nanorods were prepared through a seeding growth method, using ZnO seeds in a solution (100 mL) of Zn(NO₃)₂·6H₂O (10 mM) and hexamethylenetetramine (HTMA) (10 mM). The suspension was then heated to 90 °C for 6 h in an oil bath.

ZnO nanorods were dispersed into a thioacetamide solution (100 mL) and put into an oil bath at 60 °C for 6 h for the sulfidation of ZnO nanorods into ZnS/ZnO composites. The obtained ZnS/ZnO nanorods were washed and re-dispersed into Cd(OAc)₂·2H₂O at 60 °C for 6 h for the formation of CdS/ZnO nanorod composites. The Zn content in a pristine ZnO nanorod was set as 1 mmol. Then the ratio of Cd(OAc)₂·2H₂O was set as 0, 0.1, 0.2, 0.3, 0.4 or 0.5 mmol, corresponding to the *x* values in the P(*z*)/C(*x*)/Z/W(*y*) samples being 0, 0.2, 0.4, 0.6, 0.8 or 1.0. CdS was prepared *via* heating a solution of Cd(OAc)₂·2H₂O (10 mM) and thioacetamide (10 mM) at 60 °C for 6 h.

Preparation of ZnO seed/WS₂ composites. In a typical process, 10 mg of Zn(OAc)₂·2H₂O, 10 mg of LiOH and a certain

amount of WS₂ were added into 50 mL of ethanol under stirring for 10 min. After that, the mixture was put into a sonic bath (200 W) for 2 h. Then, the solids were washed with 75 mL of deionized water three times, and collected for the next step. The weight of WS₂ was 0, 5, 10, 15 or 20 mg, corresponding to the *y* values in the P(*z*)/C(*x*)/Z/W(*y*) samples being 0, 5, 10, 15, 20.

Preparation of ZnO nanorod/WS₂ composites. The obtained ZnO seed/WS₂ composite from the previous step was dispersed into a solution (100 mL) of Zn(NO₃)₂·6H₂O (10 mM) and hexamethylenetetramine (10 mM). Then, the suspension was put into an oil bath at 90 °C for 6 h. The product was washed and collected for the next step.

Preparation of ZnS/ZnO nanorod/WS₂ and CdS/ZnO nanorod/WS₂ composites, and CdS/WS₂ composites. The ZnO nanorod/WS₂ composite was dispersed into a certain concentration of thioacetamide solution (100 mL) and put into an oil bath at 60 °C for 6 h for the sulfidation of ZnO nanorods into ZnS/ZnO nanorod/WS₂ composites. The as-obtained ZnS/ZnO nanorod/WS₂ was washed and re-dispersed into a certain concentration of Cd(OAc)₂·2H₂O at 60 °C for 6 h for the formation of CdS/ZnO nanorod/WS₂ composites. The procedure for the preparation of CdS/WS₂ composites is similar to that for the preparation of CdS/ZnO nanorod/WS₂ composites with the concentrations of both thioacetamide and Cd(OAc)₂·2H₂O being 15 mM.

Preparation of PEDOT:PSS/CdS/ZnO/WS₂. 50 mg of the as-prepared CdS/ZnO nanorod/WS₂ composite was first sonically suspended in 5 mL of water for 10 min. Then a certain volume of PEDOT:PSS solution (1.6 wt%) was added into the suspension and stirred for 30 min to maintain the full adsorption of PEDOT:PSS. The weight ratios of PEDOT:PSS were set as 0, 0.5, 1.0, 1.5 or 2.0 in the CdS/ZnO nanorod/WS₂ composite, corresponding to the *z* value in the P(*z*)/C(*x*)/Z/W(*y*) samples being 0, 0.5, 1.0, 1.5 or 2.0. Finally, the suspension was filtered, washed with water and ethanol, and dried at 60 °C.

Characterization

The crystal structures of the samples were characterized with a powder X-ray diffractometer (XRD, Rigaku D/max-2000) using Cu-K α radiation ($\lambda = 0.15406$ nm, 45 kV, 50 mA). A transmission electron microscope equipped with an EDX system (TEM, FEI Tecnai G2) working at 300 kV was employed to observe the morphologies and characterize the chemical compositions of the samples. UV-vis diffuse reflectance spectra were recorded on a spectrophotometer (UH-4150, HITACHI) using Ba₂SO₄ as a reference. The UV-vis absorption spectra of PEDOT:PSS were collected on a UH5300 (HITACHI) spectrophotometer. The photoluminescence (PL) measurements were carried out at room temperature with a luminescence spectrometer (PerkinElmer, LS-55) using 325 nm as the excitation wavelength. Time-resolved PL spectra were recorded on a FluoroMax@-4 Fluorescence Spectrophotometer from HORIBA Scientific under 301 nm excitation at room temperature. The Raman spectra were obtained with a MODEL BX41TF Raman system, using an excitation source of 532 nm. Infrared (IR) spectra were recorded with a FTIR spectrometer (Shi-madzu) over the range of 400–4000 cm⁻¹ in the form of KBr pellets.

Photocatalytic reactions

Photocatalytic H₂ evolution. The photocatalytic reaction was performed in a closed gas-circulation system with a side window. The photocatalyst powder (15 mg) was dispersed ultrasonically in an aqueous solution (300 mL) containing Na₂S (0.2 M) and Na₂SO₃ (0.3 M) for 10 min. The reaction was carried out by irradiating the suspension with light from a 300 W Xe lamp (PLS-SXE300/300UV) equipped with an AM 1.5G filter (100 mW cm⁻²). The amount of produced H₂ was measured using gas chromatography (Agilent 7890A) with a thermal conductivity detector (TCD). Photocatalytic reactions at 500, 550, 600 and 700 nm were carried out using the light from a $\lambda > 400$ nm cut-off and the corresponding band-pass filters ($\Delta\lambda = \pm 15$ nm) (Fig. S18†).

The apparent quantum yields (AQY) for hydrogen evolution were measured under the similar experimental conditions, except for the addition of band-pass filters. The apparent quantum yields are defined *via* the following equations:

$$\begin{aligned} \text{AQY}(\%) &= \frac{\text{number of reacted electrons}}{\text{number of incident photons}} \times 100 \\ &= \frac{2 \times \text{number of H}_2 \text{ molecules evolved}}{\text{number of incident photons}} \times 100 \end{aligned}$$

The number of incident photons was measured using a radiometer (Photoelectric Instrument Factory, Beijing Normal University).

Pt and PdS deposition experiments

The Pt loaded C(0.6)/Z sample was prepared through a similar procedure to that used for the photocatalytic H₂ evolution, with the addition of 0.1 mL of H₂PtCl₆ (Pt content 1.5 mg mL⁻¹) into the reaction suspensions. Then the suspension was irradiated with light from a 300 W Xe lamp (PLS-SXE300/300UV) for 0.5 h before the photocatalytic H₂ evolution test.

The loading of PdS on C(0.6)/Z/W(10) was realized *via in situ* deposition. 0.072 mL of PdCl₂ aqueous solution (Pd content 1.5 mg mL⁻¹) was added dropwise into a suspension of C(0.6)/Z/W(10) powder (15 mg) dispersed in Na₂S aqueous solution (0.2 M) just before the photocatalytic reaction.

Photoelectrochemical characterization

The photoelectrochemical measurements were carried out using a standard three-electrode cell with an Ag/AgCl (3.0 M KCl) reference electrode and platinum foil as a counter electrode on an Autolab PGSTAT302N (ECO-Chemie) electrochemical workstation. Na₂S (0.2 mol L⁻¹) and Na₂SO₃ (0.3 mol L⁻¹) were used as the electrolyte. The working electrodes were prepared *via* the spin coating method with 10 mg of sample on 20 mm × 20 mm fluorine doped tin oxide (FTO) glass. All linear sweep voltammograms were measured at a scan rate of 10 mV s⁻¹. Photocurrent curves were measured using a 0.0 V bias (*vs.* Ag/AgCl) under simulated sunlight irradiation. Photocurrent curves at 500, 550, 600 and 700 nm were measured using a $\lambda > 400$ nm cut-off and the corresponding band-pass filters ($\Delta\lambda = \pm 15$ nm). AC impedance measurements were carried out using

a 5.0 mV AC voltage signal over the 100 kHz to 1 Hz frequency range.

Acknowledgements

This work was financially supported by projects of the Natural Science Foundation of China (21471040, 21271055 and 21501035). We acknowledge support from the Program for Innovation Research of Science in the Harbin Institute of Technology (PIRS of HIT B201508).

Notes and references

- X. Chen, S. Shen, L. Guo and S. S. Mao, *Chem. Rev.*, 2010, **110**, 6503–6570.
- J. Liu, Y. Liu, N. Liu, Y. Han, X. Zhang, H. Huang, Y. Lifshitz, S. T. Lee, J. Zhong and Z. Kang, *Science*, 2015, **347**, 970–974.
- C. Pan, T. Takata, M. Nakabayashi, T. Matsumoto, N. Shibata, Y. Ikuhara and K. Domen, *Angew. Chem., Int. Ed.*, 2015, **54**, 2955–2959.
- L. Liao, Q. Zhang, Z. Su, Z. Zhao, Y. Wang, Y. Li, X. Lu, D. Wei, G. Feng, Q. Yu, X. Cai, J. Zhao, Z. Ren, H. Fang, F. Robles-Hernandez, S. Baldelli and J. Bao, *Nat. Nanotechnol.*, 2014, **9**, 69–73.
- T. H. Lee, S. Y. Kim and H. W. Jang, *Nanomaterials*, 2016, **6**, 194.
- P. Zhang, T. Wang, X. Chang and J. Gong, *Acc. Chem. Res.*, 2016, **49**, 911–921.
- S. Bai, J. Jiang, Q. Zhang and Y. Xiong, *Chem. Soc. Rev.*, 2015, **44**, 2893–2939.
- P. Zhou, J. Yu and M. Jaroniec, *Adv. Mater.*, 2014, **26**, 4920–4935.
- H. Li, Y. Zhou, W. Tu, J. Ye and Z. Zou, *Adv. Funct. Mater.*, 2015, 998–1013.
- L. Mu, Y. Zhao, A. Li, S. Wang, Z. Wang, J. Yang, Y. Wang, T. Liu, R. Chen, J. Zhu, F. Fan, R. Li and C. Li, *Energy Environ. Sci.*, 2016, **9**, 2463–2469.
- J. Zhu, F. Fan, R. Chen, H. An, Z. Feng and C. Li, *Angew. Chem., Int. Ed.*, 2015, **54**, 9111–9114.
- Y. Zhou, G. Chen, Y. Yu, L. Zhao, J. Sun, F. He and H. Dong, *Appl. Catal., B*, 2016, **183**, 176–184.
- D. Wang, T. Hisatomi, T. Takata, C. Pan, M. Katayama, J. Kubota and K. Domen, *Angew. Chem., Int. Ed.*, 2013, **52**, 11252–11256.
- R. Li, F. Zhang, D. Wang, J. Yang, M. Li, J. Zhu, X. Zhou, H. Han and C. Li, *Nat. Commun.*, 2013, **4**, 1432.
- R. Marschall, *Adv. Funct. Mater.*, 2014, **24**, 2421–2440.
- H. Pan, *Renewable Sustainable Energy Rev.*, 2016, **57**, 584–601.
- X. Chen, Z. Zhang, L. Chi, A. K. Nair, W. Shangguan and Z. Jiang, *Nano-Micro Lett.*, 2015, **8**, 1–12.
- T.-T. Zhuang, Y. Liu, Y. Li, Y. Zhao, L. Wu, J. Jiang and S.-H. Yu, *Angew. Chem., Int. Ed.*, 2016, **128**, 6506–6510.
- T. T. Zhuang, Y. Liu, Y. Li, M. Sun, Z. J. Sun, P. W. Du, J. Jiang and S. H. Yu, *Small*, 2017, **13**, 1602629.
- Y. Hou, B. L. Abrams, P. C. Vesborg, M. E. Bjorketun, K. Herbst, L. Bech, A. M. Setti, C. D. Damsgaard, T. Pedersen, O. Hansen, J. Rossmeisl, S. Dahl,

- J. K. Norskov and I. Chorkendorff, *Nat. Mater.*, 2011, **10**, 434–438.
- 21 Y. Yang, J. Gu, J. L. Young, E. M. Miller, J. A. Turner, N. R. Neale and M. C. Beard, *Science*, 2015, **350**, 1061–1065.
- 22 W. Wang, H. Wang, Q. Zhu, W. Qin, G. Han, J. R. Shen, X. Zong and C. Li, *Angew. Chem., Int. Ed.*, 2016, **55**, 9229–9233.
- 23 M. Zhong, T. Hisatomi, Y. Kuang, J. Zhao, M. Liu, A. Iwase, Q. Jia, H. Nishiyama, T. Minegishi, M. Nakabayashi, N. Shibata, R. Niishiro, C. Katayama, H. Shibano, M. Katayama, A. Kudo, T. Yamada and K. Domen, *J. Am. Chem. Soc.*, 2015, **137**, 5053–5060.
- 24 M. Zhong, T. Hisatomi, Y. Sasaki, S. Suzuki, K. Teshima, M. Nakabayashi, N. Shibata, H. Nishiyama, M. Katayama, T. Yamada and K. Domen, *Angew. Chem., Int. Ed.*, 2017, **129**, 4817–4821.
- 25 Y. Qu, L. Liao, R. Cheng, Y. Wang, Y. C. Lin, Y. Huang and X. Duan, *Nano Lett.*, 2010, **10**, 1941–1949.
- 26 B. Mahler, V. Hoepfner, K. Liao and G. A. Ozin, *J. Am. Chem. Soc.*, 2014, **136**, 14121–14127.
- 27 X. Zong, J. Han, G. Ma, H. Yan, G. Wu and C. Li, *J. Phys. Chem. C*, 2011, **115**, 12202–12208.
- 28 Q. Xiang, F. Cheng and D. Lang, *ChemSusChem*, 2016, **9**, 996–1002.
- 29 Y. Sang, Z. Zhao, M. Zhao, P. Hao, Y. Leng and H. Liu, *Adv. Mater.*, 2015, **27**, 363–369.
- 30 F. Raza, J. H. Park, H.-R. Lee, H.-I. Kim, S.-J. Jeon and J.-H. Kim, *ACS Catal.*, 2016, **6**, 2754–2759.
- 31 G. Li, R. Zhu and Y. Yang, *Nat. Photonics*, 2012, **6**, 153–161.
- 32 S. Bai, W. Jiang, Z. Li and Y. Xiong, *ChemNanoMat*, 2015, **1**, 223–239.
- 33 J. Lee and W. Choi, *J. Electrochem. Soc.*, 2015, **162**, A935–A939.
- 34 L. Groenendaal, F. Jonas, D. Freitag, H. Pielartzik and J. R. Reynolds, *Adv. Mater.*, 2000, **12**, 481–494.
- 35 J. Yang, H. Yan, X. Wang, F. Wen, Z. Wang, D. Fan, J. Shi and C. Li, *J. Catal.*, 2012, **290**, 151–157.
- 36 Y. Liu, Z. Kang, H. Si, P. Li, S. Cao, S. Liu, Y. Li, S. Zhang, Z. Zhang, Q. Liao, L. Wang and Y. Zhang, *Nano Energy*, 2017, **35**, 189–198.
- 37 S. Cao, X. Yan, Z. Kang, Q. Liang, X. Liao and Y. Zhang, *Nano Energy*, 2016, **24**, 25–31.
- 38 Z. Bai, X. Yan, Y. Li, Z. Kang, S. Cao and Y. Zhang, *Adv. Energy Mater.*, 2016, **6**, 1501459.